Variational Approach for Restoring Blurred Images with Cauchy Noise

Sciacchitano, Federica; Dong, Yiqiu; Zeng, Tieyong

Published in:
SIAM Journal on Imaging Sciences

DOI:
10.1137/140997816

Published: 17/09/2015

Document Version:
Publisher's PDF, also known as Version of record

SIAM J. IMAGING SCIENCES
Vol. 8, No. 3, pp. 1894–1922

Variational Approach for Restoring Blurred Images with Cauchy Noise*

Federica Sciacchitano†, Yiqiu Dong†, and Tieyong Zeng‡

Abstract. The restoration of images degraded by blurring and noise is one of the most important tasks in image processing. In this paper, based on the total variation (TV) we propose a new variational method for recovering images degraded by Cauchy noise and blurring. In order to obtain a strictly convex model, we add a quadratic penalty term, which guarantees the uniqueness of the solution. Due to the convexity of our model, the primal dual algorithm is employed to solve the minimization problem. Experimental results show the effectiveness of the proposed method for simultaneously deblurring and denoising images corrupted by Cauchy noise. Comparison with other existing and well-known methods is provided as well.

Key words. Cauchy noise, image deblurring, image denoising, primal dual algorithm, total variation regularization, variational model

AMS subject classifications. 68U10, 94A08, 49J40, 52A41, 65K10, 90C47, 35B45

DOI. 10.1137/140997816

1. Introduction.

Image deblurring and image denoising are fundamental problems in the applied mathematics community; see, for instance, [4, 5]. Most of the literature deals with the restoration of images corrupted by additive Gaussian noise [10, 15, 22, 54, 60]. Unfortunately, in many engineering applications the noise has a very impulsive character, and thus it cannot be modeled by this kind of noise. The most common example of impulsive noise is given by the impulse noise [12, 45, 46], which can be caused, for instance, by analogue-to-digital converter errors, by malfunctioning pixel elements in the camera sensors, and so on. Another impulsive degradation is given by Cauchy noise, which appears frequently in atmospheric and underwater acoustic noises, radar and sonar applications, air turbulence, wireless communication systems, biomedical images, and synthetic aperture radar (SAR) images. For an overview we refer the reader to [36, 39, 40, 49, 50, 52] and references therein.

Mathematically speaking, the degraded image f in the presence of blurring and Cauchy noise is given by $f = Ku + v$, where u is the original image defined on the image domain $\Omega \subset \mathbb{R}^2$, K is the blurring operator, and v is some Cauchy noise. A random variable V follows the Cauchy distribution if it has density

$$g(v) = \frac{1}{\pi} \frac{\gamma}{\gamma^2 + (v - \delta)^2}, \tag{1.1}$$

*Received by the editors December 1, 2014; accepted for publication (in revised form) July 6, 2015; published electronically September 17, 2015.
http://www.siam.org/journals/siims/8-3/99781.html
†Department of Applied Mathematics and Computer Science, Technical University of Denmark, 2800 Kgs. Lyngby, Denmark (feds@dtu.dk, yido@dtu.dk). The work of the second author was supported by Advanced Grant 291405 from the European Research Council.
‡Department of Mathematics, Hong Kong Baptist University, Kowloon Tong, Hong Kong (zeng@hkbu.edu.hk). The work of this author was partially supported by NSFC 11271049, RGC 211911, 12302714, and RFGs of HKBU.

where $\gamma > 0$ is the scale parameter and $\delta \in \mathbb{R}$ is called the localization parameter. The scale parameter determines the spread of the distribution around δ and plays a role similar to that of the variance in the Gaussian distribution, while the localization parameter corresponds to the median of the distribution.

Recently, several approaches have been proposed to deal with Cauchy noise; for instance, Chang et al. [16] used recursive Markov random field models for reconstructing images under Cauchy noise. Achim and Kuruoğlu [1] proposed a method for denoising a image degraded by Cauchy noise in the complex wavelet domain. Wan, Canagarajah, and Achim [59] studied a segmentation technique for noisy color images corrupted by Cauchy noise. As far as we know, in the literature, no one has ever studied a variational model for removing Cauchy noise. Hence, our contribution is to propose a variational model for deblurring and denoising degraded images with Cauchy noise.

One of the most famous variational models is the ROF model [54]. This approach was introduced in 1992 by Rudin, Osher, and Fatemi, and it is defined as follows:

$$\inf_{u \in BV(\Omega)} J(u) + \frac{\lambda}{2} \int_{\Omega} (f-u)^2 \mathrm{d}x, \tag{1.2}$$

where $J(u) = \int_{\Omega} |Du|$ is the total variation (TV) regularization term, BV is the space of the functions of bounded variation (see [4] or below), the last term is the data fidelity term, and $\lambda > 0$ is the regularization parameter, which represents the trade-off between a good fit of f and a smoothness due to the TV regularization term. Due to its capability of preserving sharp edges, it is a very successful and popular approach for denoising images corrupted by additive Gaussian noise.

Over the years, many variational models based on TV have been introduced for removing other noises, such as multiplicative noise [3, 21, 53], impulse noise [12, 46, 62], Poisson noise [19, 24, 41, 51, 56], etc. In our work, inspired by the above studies, we introduce a variational model, based on TV as the regularization term, for restoring images with blur and Cauchy noise. In particular, we propose the following problem for removing Cauchy noise:

$$\inf_{u \in BV(\Omega)} J(u) + \frac{\lambda}{2} \int_{\Omega} \log\Big(\gamma^2 + (u-f)^2\Big) \mathrm{d}x, \tag{1.3}$$

where $\gamma > 0$ is the scale parameter; see (1.1). As one can see, we keep the same regularization term as in the ROF model, but we adapt the data fidelity term to the Cauchy noise, introducing one that is suitable for such a type of noise. We emphasize that TV regularization is a very useful tool for preserving edges but is not so good for texture recovery; thus, clearly, the proposed model can be extended to other modern regularization terms such as nonlocal TV [26, 58, 63], high order TV [61], dictionary learning [22, 33], or a tight-frame approach [8, 38].

Unfortunately, since the data fidelity term is not convex, the restored results depend on the initialization and the numerical scheme. Hence, to overcome this problem we use a quadratic penalty function technique; in particular, we introduce the following minimization problem:

$$\inf_{u \in BV(\Omega)} J(u) + \frac{\lambda}{2} \left(\int_{\Omega} \log\Big(\gamma^2 + (u-f)^2\Big) \mathrm{d}x + \mu \|u - u_0\|_2^2 \right), \tag{1.4}$$

where u_0 is the image obtained by applying the median filter [5] to the noisy image. Under some assumptions on μ, we are able to prove that (1.4) is convex and there exists a unique solution of (1.4). We employ the median filter in the quadratic penalty term, since it has been shown that it works well for removing impulse noise [12], and the Cauchy degradation has some similarities with the impulse degradation.

Readily, we can also generalize our model for restoring a blurred image corrupted by Cauchy noise. Given a linear blurring operator K, we consider the following convex model for deblurring and denoising simultaneously:

$$\inf_{u\in BV(\Omega)} J(u) + \frac{\lambda}{2}\left(\int_\Omega \log\left(\gamma^2 + (Ku-f)^2\right)\mathrm{d}x + \mu\|Ku-u_0\|_2^2\right). \tag{1.5}$$

The minimization problem in (1.5) could be solved by the primal dual algorithm proposed by Chambolle and Pock in [11] or other efficient optimization algorithms [14, 17, 26, 61, 62].

Numerical results show the potential and the effectiveness of the proposed method for restoring blurred images degraded by Cauchy noise. Furthermore, we compare the reconstructed images obtained by our method with those given by the ROF model [54], the median filter [25], the myriad filter [29], the BM3D [18], the SURE-LET [43], the wavelet shrinkage [5], and the L^1-TV model [46].

The rest of the paper is organized as follows. In section 2, we describe the alpha-stable distribution, focusing on the Cauchy distribution. Using the MAP estimator, in section 3 we derive our model for simultaneously deblurring and denoising an image and we analyze some theoretical properties of this model. Adding a quadratic penalty term, which depends on the median filter, in section 4, we propose a convex model to restore blurred and degraded images by Cauchy noise and we prove the existence and uniqueness of the solution. In section 5, using the primal dual algorithm, we show some numerical results and we compare them with the reconstructions obtained with other existing approaches. Finally, in section 6, we draw some conclusions.

2. Cauchy noise modeling.

Many studies in image and signal processing rely on the fundamental assumption that the noise follows a Gaussian distribution. This hypothesis is justified due to the existence of the central limit theorem; see [31]. Unfortunately, most of the real world problems cannot be modeled by Gaussian distribution, since the noise is much more impulsive than the one that is modeled by additive Gaussian noise. Examples of these applications can be found in the radar and sonar applications, where there are atmospheric and underwater acoustic noises, in biomedical images, in SAR images, and so on. These types of noise follow the so called alpha-stable distributions [47, 48, 55].

The alpha-stable distributions are closed under additions; i.e., the sum of two alpha-stable random variables is still an alpha-stable random variable. Moreover, the alpha-stable random variables obey to the generalized central limit theorem [48]. But, this class of random variables has no close formula for densities and distribution functions (apart from Gaussian, Cauchy, and Lévy distributions). The distributions of this class are all bell-shaped, with increasing density on the left and decreasing density on the right. The heaviness of the distribution tails is controlled by the parameter $\alpha \in (0, 2]$; i.e., the tails grow thicker as α becomes smaller.

In Figure 1, we show the probability density functions (PDFs) of alpha-stable distributions with different values of α. The distribution with $\alpha = 2$ corresponds to the well-known Gaussian

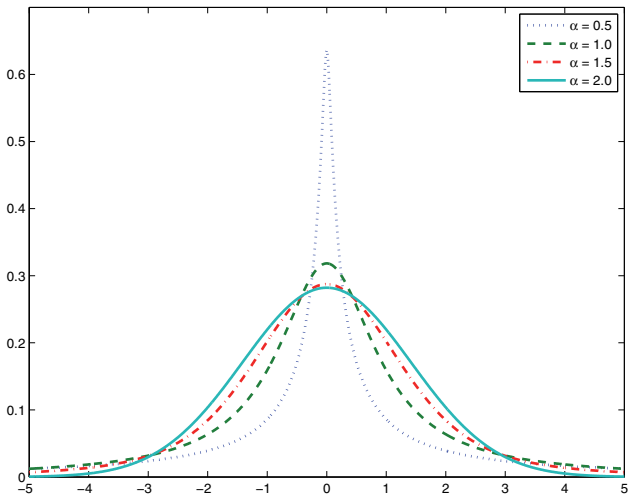

Figure 1. *Comparison of the PDFs of alpha-stable distributions with* $\alpha = 0.5$, $\alpha = 1$, $\alpha = 1.5$, *and* $\alpha = 2$.

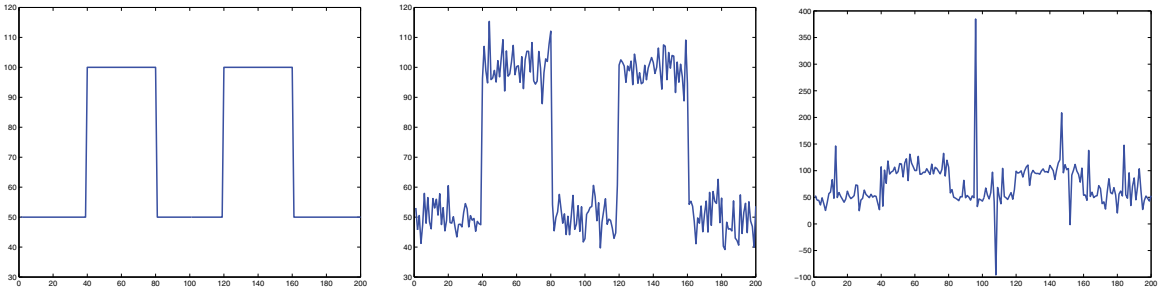

(a) Noise free signal. (b) Degraded by Gaussian noise. (c) Degraded by Cauchy noise.

Figure 2. *Alpha-stable noise in one dimension: notice that the y-axis has different scales (scale between* 30 *and* 120 *on* (a) *and* (b) *and* -100 *and* 400 *on* (c)*).* (a) *one-dimensional noise-free signal;* (b) *signal degraded by an additive Gaussian noise;* (c) *signal degraded by an additive Cauchy noise. The Cauchy noise is more impulsive than the Gaussian noise.*

distribution, and the one with $\alpha = 1$ corresponds to the Cauchy distribution. Comparing the PDFs, we see that the tails of the bells become heavier as α decreases. In fact, the Cauchy bell ($\alpha = 1$) has a thicker tail than the Gaussian distribution ($\alpha = 2$). Thus, the rare events have more probability of occurring in the Cauchy bell curve than in the Gaussian bell curve, and for this reason, the noise generated from the Cauchy distribution is more impulsive than the Gaussian one. For instance, the Cauchy noise can contain powerful noise spikes that can be more than a hundred times the magnitude of the humbler Gaussian noise spikes.

In order to illustrate the difference between the Gaussian noise and the Cauchy noise, in Figure 2 we show a one-dimensional noise-free signal and the corresponding degraded signal by the Gaussian noise and the Cauchy noise. The noisy signal corrupted by the Gaussian noise has been obtained simply by adding random values from a Gaussian distribution. From [47, 48], we know that the Cauchy noise can be obtained from the ratio of two independent Gaussian variables. Hence, to create the noisy signal with the Cauchy noise, first we generate two vectors

containing random values from the Gaussian distribution, and then we add the ratio between these two vectors to the original signal. From the figures, one can see that the Cauchy noise is much more impulsive than the Gaussian noise, since the rare events have more probability to occur. Note that the vertical scale goes from 30 to 120 for the original signal and the one degraded by the Gaussian noise, while it goes from -100 to 400 for the signal degraded by the Cauchy noise.

Finally, we now describe how Cauchy noise influences the clean image. Given the original image $u : \Omega \to \mathbb{R}$, with $\Omega \subset \mathbb{R}^2$ being a bounded, open, and connected set with compact Lipschitz boundary, the noisy image $f : \Omega \to \mathbb{R}$ is given by

$$f = u + v,$$

where v represents the random noise that models a Cauchy distribution. A random variable V follows the Cauchy distribution, $V \sim \text{Cauchy}(\gamma, \delta)$, if it has density as in (1.1). Without loss of generality, from now on, in our analysis we consider $\delta = 0$.

3. Variational model.

In this section we analyze a variational model for deblurring and denoising images corrupted by Cauchy noise. In the first part, we focus only on the denoising case and using the maximum a posteriori (MAP) estimator (see [31]) to derive a variational model. Then, we study some properties of the restoration model, i.e., the existence of a minimizer and the minimum maximum principle. Later, we incorporate a blurring operator K in our variational model for simultaneously deblurring and denoising an image corrupted by Cauchy noise.

3.1. Variational model via MAP estimator.

Our goal is to find a variational model to restore an image corrupted by Cauchy noise; in particular, we want to recover the original image u, given the noisy image $f = u + v$, where v follows the Cauchy noise. Based on [3], we derive our model using the Bayes rule and the MAP estimator; see [31]. In the following, we denote the random variables with the uppercase letters F, U, and V, the respective instances with the lowercase letters f, u, and v, and the respective density functions with g_F, g_U, and g_V.

As already said in the previous section, we assume that v follows a "zero-centered" Cauchy law, and thus its density function is defined as follows:

$$g_V(v) = \frac{1}{\pi} \frac{\gamma}{\gamma^2 + v^2}.$$

Given the noisy image F, for restoring the original image U, we have to maximize the conditional probability $P(U|F)$. From Bayes's rule [31], we know that

$$P(U|F) = \frac{P(F|U)P(U)}{P(F)}. \tag{3.1}$$

Based on (3.1), we can equivalently minimize

$$-\log(P(U|F)) = -\log(P(F|U)) - \log(P(U)) + \log(P(F)). \tag{3.2}$$

Since the quantity $P(F)$ is constant with respect to the variable U, we just need to minimize $-\log(P(F|U)) - \log(P(U))$.

The pixels of our image are corrupted by Cauchy noise; thus for $x \in \Omega$, with Ω the set of the pixels of the image, we have

$$P(f(x)|u(x)) = P_{u(x)}(f(x)) = \frac{\gamma}{\pi\big(\gamma^2 + (u(x) - f(x))^2\big)}.$$

Inspired by [3], we assume that U follows a Gibbs prior:

$$g_U(u) = \frac{1}{Z}\exp(-\beta J(u)),$$

where Z is the normalization factor, $\beta > 0$, and J is a nonnegative given function such as $J(u) = \int_\Omega |Du|$ (the notation will be explained in the next section).

Now, since the pixels $x \in \Omega$ are mutually independent and identically distributed (i.i.d.), we have $P(U) = \prod_{x\in\Omega} P(U(x))$, where $U(x)$ is the instance of the random variable U at the pixels x. Hence, minimizing (3.2) is equivalent to minimizing

$$-\log(P(F|U)) = -\int_\Omega \Big(\log\big(P(F(x)|U(x))\big) + \log\big(P(U(x))\big)\Big). \tag{3.3}$$

Substituting the explicit expressions of $\log P(F(x)|U(x))$ and $\log P(U(x))$ in (3.3), we can easily write (3.3) as follows:

$$-\log(P(F|U)) = \int_\Omega \Big(\log\big(\gamma^2 + (U(x) - F(x))^2\big) + \beta J(U(x)) + \log\pi + \log Z - \log\gamma\Big). \tag{3.4}$$

Since the last three terms are constants, our model for restoring images corrupted with Cauchy noise is given by

$$\inf_{u\in BV(\Omega)} E(u) := \int_\Omega |Du| + \frac{\lambda}{2}\int_\Omega \log\Big(\gamma^2 + (u - f)^2\Big)\mathrm{d}x, \tag{3.5}$$

where $\lambda = \frac{2}{\beta}$ is a strictly positive parameter and we assume $f \in L^\infty(\Omega)$.

As in [3, 21, 54], in our work we consider the recovered image u in the space of the functions of bounded variation (BV). In particular, $u \in BV(\Omega)$ iff $u \in L^1(\Omega)$ and the seminorm in the space $BV(\Omega)$ is finite, where the BV-seminorm is defined as follows:

$$\int_\Omega |Du| := \sup\left\{\int_\Omega u \cdot \mathrm{div}(\xi(x))\mathrm{d}x \,\middle|\, \xi \in C_0^\infty(\Omega, \mathbb{R}^2), \|\xi\|_{L^\infty(\Omega,\mathbb{R}^2)} \le 1\right\}. \tag{3.6}$$

The space $BV(\Omega)$ endowed with the norm $\|u\|_{BV} = \|u\|_{L^1} + \int_\Omega |Du|$ is a Banach space. If $u \in BV(\Omega)$, (3.6) corresponds to the TV. From the compactness of the space $BV(\Omega)$, we have the following embedding, $BV(\Omega) \hookrightarrow L^p(\Omega)$, with $1 \le p \le 2$, and for $p < 2$ it is compact (see [2, 3] for more explanations).

In the following section, we give some theoretical results on the existence of the minimizer and we enunciate the minimum-maximum principle.

3.2. Properties of the model (3.5). We start this section with proving that there exists at least one solution for the minimization problem (3.5).

Theorem 3.1. *Let f be in $L^\infty(\Omega)$; then the problem (3.5) has at least one solution in $BV(\Omega)$ satisfying*

$$\inf_\Omega f \le u \le \sup_\Omega f.$$

Proof. Let us denote $a = \inf f$ and $b = \sup f$, and consider a minimizing sequence $\{u_n\} \in BV(\Omega)$ for (3.5). First of all, we show that we can assume $a \le u_n \le b$ without loss of generality, and so the sequence $\{u_n\}$ is bounded in $L^1(\Omega)$. Fixing $x \in \Omega$ and denoting the data fidelity term with $h : \mathbb{R} \to \mathbb{R}$, where $h(t) := \log(\gamma^2 + (t - f(x))^2)$, we have

$$h'(t) = \frac{2\big(t - f(x)\big)}{\gamma^2 + \big(t - f(x)\big)^2}.$$

Thus, the function h is decreasing if $t < f(x)$ and increasing if $t > f(x)$. For every $M \ge f(x)$, we have

$$h(\min(t, M)) \le h(t).$$

Hence, if $M = b$, we have

$$\int_\Omega \log\Big(\gamma^2 + \big(\inf(t, b) - f(x)\big)^2\Big)\mathrm{d}x \le \int_\Omega \log\Big(\gamma^2 + \big(t - f(x)\big)^2\Big)\mathrm{d}x.$$

Furthermore, from [34], we know that $\int |D \inf(u, b)| \le \int |Du|$. By definition of our functional E, we can conclude that $E(\inf(u, b)) \le E(u)$. In the same way, we can prove that $E(\sup(u, a)) \le E(u)$, with $a = \inf f$. Hence, since $a \le u_n \le b$, the sequence $\{u_n\}$ is bounded in $L^1(\Omega)$.

Now, applying our functional E in (3.5) to the sequence $\{u_n\}$, we have that $E(u_n)$ is bounded. In particular, there exists a constant $C > 0$ such that $E(u_n) \le C$. The data fidelity term has minimum value $2 \log \gamma$ when $u = f$ and $E(u_n)$ is bounded, and hence the regularization term $\int |D(u_n)|$ is also bounded. Thus, the sequence $\{u_n\}$ is bounded in $BV(\Omega)$ and there exists $u \in BV(\Omega)$ such that up to a subsequence, we have $u_n \to u$ in $BV(\Omega)$-weak and $u_n \to u$ in $L^1(\Omega)$-strong. Furthermore, using $a \le u \le b$, the lower semicontinuity of the TV, and Fatou's lemma, we have that u is a minimizer of the problem (3.5). Remark that if $\gamma \ge 1$, we can directly apply Fatou's lemma, since the logarithm does not take negative values; if $\gamma < 1$, we can still use Fatou's lemma, but we need some considerations. In fact, letting $u = \gamma v$ and $f = \gamma f_0$ (with $v \in BV(\Omega)$ and $f_0 \in L^\infty(\Omega)$), the minimization problem in (3.5) can be rewritten as follows:

$$\inf_{v \in BV(\Omega)} E(v) := \gamma \int_\Omega |Dv| + \frac{\lambda}{2} \int_\Omega \log\Big(1 + (v - f_0)^2\Big)\mathrm{d}x.$$

Hence, also in the case $\gamma < 1$, the logarithm does not take negative values, and then the use of Fatou's lemma is ensured. ∎

Now we are able to prove, under some hypothesis, that there exists a unique solution for our minimization problem (3.5).

Proposition 3.2. *Let f be in $L^\infty(\Omega)$; then the problem (3.5) has only one solution u such that $f - \gamma < u < f + \gamma$.*

Proof. Using the same notation as before and fixing $x \in \Omega$, we have

$$h''(t) = \frac{2\big(\gamma^2 - (t - f(x))^2\big)}{\big(\gamma^2 + (t - f(x))^2\big)^2},$$

where $t \in \mathbb{R}$. If $f - \gamma < t < f + \gamma$, the function h is strictly convex, and hence there exists a unique minimizer for the problem defined in (3.5). ∎

In the following proposition we enunciate the minimum-maximum principle.

Proposition 3.3. *Let f_1 and f_2 be in $L^\infty(\Omega)$, with $a_1 = \inf_\Omega f_1$, $a_2 = \inf_\Omega f_2$, $b_1 = \sup_\Omega f_1$, and $b_2 = \sup_\Omega f_2$. Let us assume that $f_1 < f_2$. Then, denoting with u_1 (resp., u_2) a solution of (3.5) for $f = f_1$ (resp., $f = f_2$), we have $u_1 \le u_2$ if $b_2 < \gamma + a_1$.*

Proof. From Theorem 3.1, we know that problem (3.5) admits solutions. Thus, by definition of u_1 and u_2 we have

$$J(u_1 \wedge u_2) + \frac{\lambda}{2}\int_\Omega \log(\gamma^2 + (u_1 \wedge u_2 - f_1)^2)\mathrm{d}x \ge J(u_1) + \frac{\lambda}{2}\int_\Omega \log(\gamma^2 + (u_1 - f_1)^2)\mathrm{d}x$$

and

$$J(u_1 \vee u_2) + \frac{\lambda}{2}\int_\Omega \log(\gamma^2 + (u_1 \vee u_2 - f_2)^2)\mathrm{d}x \ge J(u_2) + \frac{\lambda}{2}\int_\Omega \log(\gamma^2 + (u_2 - f_2)^2)\mathrm{d}x,$$

where $u_1 \wedge u_2 = \inf(u_1, u_2)$ and $u_1 \vee u_2 = \sup(u_1, u_2)$. From [9, 27], we know that $J(u_1 \wedge u_2) + J(u_1 \vee u_2) \le J(u_1) + J(u_2)$; thus, adding the two inequalities above we have

$$\int_\Omega \Big(\log(\gamma^2 + (u_1 \wedge u_2 - f_1)^2) - \log(\gamma^2 + (u_1 - f_1)^2) + \log(\gamma^2 + (u_1 \vee u_2 - f_2)^2) - \log(\gamma^2 + (u_2 - f_2)^2)\Big)\mathrm{d}x \ge 0.$$

We now split the domain Ω into two parts $\Omega = \{u_1 > u_2\} \cup \{u_1 \le u_2\}$ and deduce that

(3.7)
$$\int_{\{u_1 > u_2\}} \Big(\log(\gamma^2 + (u_2 - f_1)^2) - \log(\gamma^2 + (u_1 - f_1)^2) + \log(\gamma^2 + (u_1 - f_2)^2) - \log(\gamma^2 + (u_2 - f_2)^2)\Big)\mathrm{d}x \ge 0.$$

With the hypothesis $b_2 < \gamma + a_1$, one can prove that the integrand of the above integral is strictly negative (for further details we refer the reader to the appendix. Hence, we have that $\{u_1 > u_2\}$ has a zero Lesbegue measure, and thus we have proved that $u_1 \le u_2$ a.e. in the domain Ω. ∎

Although we proved under some conditions that there exists a unique solution for (3.5), the model is not convex. Due to the nonconvexity of (3.5), the restored results from (3.5) strongly depend on the initialization and the numerical schemes. To overcome this problem, in section 4 we introduce a convex model by adding a quadratic penalty term. Before that we first extend (3.5) to the deblurring case.

3.3. Deblurring and denoising case. Since in the real applications the observed image f is usually not only corrupted by noise but also blurred, we extend the minimization model in (3.5) to the deblurring and denoising case. In particular, the blurred and noisy image is given by $f = Ku+v$, where $K \in \mathcal{L}(L^1(\Omega), L^2(\Omega))$ is a known linear and continuous blurring operator and $v \in L^2(\Omega)$, as above, represents the Cauchy noise. In the deblurring and denoising case, the minimization problem becomes

$$\inf_{u\in BV(\Omega)} \int_\Omega |Du| + \frac{\lambda}{2}\int_\Omega \log\Big(\gamma^2 + (Ku-f)^2\Big)\mathrm{d}x. \tag{3.8}$$

As in the denoising case, (3.8) is nonconvex; in the next section, to overcome this problem we introduce a convex model.

4. Convex variational model. In this section we introduce a convex variation model for deblurring and denoising an image corrupted by Cauchy noise. At the beginning, we focus only on the denoising case, and then we generalize the model for the deblurring case. Drawing inspiration from the nonconvex model defined in (3.5), we introduce a new model by adding a quadratic penalty term that is based on the image given by applying the median filter to the noisy image f. The reason why we choose to use the median filter will be explained in subsection 4.1.

In particular, introducing a quadratic penalty term into the previous nonconvex model (3.5), we have

$$\inf_{u\in BV(\Omega)} \int_\Omega |Du| + \frac{\lambda}{2}\left(\int_\Omega \log\Big(\gamma^2 + (u-f)^2\Big)\mathrm{d}x + \mu\|u-u_0\|_2^2\right), \tag{4.1}$$

where u_0 is the image obtained by applying the median filter to the noisy image f and $\lambda > 0$ and $\mu > 0$ are the regularization parameters. In this way, we will prove that the model, under some conditions, is strictly convex.

4.1. Median filter. In this part we explain the reason why we choose the median filter [25] as a quadratic penalty term, focusing on the analogies between the Cauchy noise and impulse noise. Due to its simplicity and its capability of preserving image edges, in past decades, the median filter has attracted much attention in image processing [7, 35, 42, 57], especially for denoising images corrupted by impulse noise; see [12, 20]. Given the original image u, the noisy image f corrupted by impulse noise is defined as follows:

$$f(x) = \begin{cases} u(x) & \text{with probability } 1-\sigma, \\ \eta & \text{with probability } \sigma, \end{cases} \quad \text{with } \ x \in \Omega,$$

where η is a uniformly distributed random variable with values in $[\min u, \max u]$ and $\sigma > 0$ is the noise level.

Figure 3(a) shows the original Parrot image, and Figures 3(b), 3(c), and 3(d), respectively, represent the images corrupted by additive Gaussian noise, impulse noise, and Cauchy noise. In Figures 3(e)–3(h) we show the zooms of the top left corners of 3(a)–3(d). One can see that the image degraded by Gaussian noise looks slightly different from the images corrupted by Cauchy noise and impulse noise, while in some way Cauchy noise and impulse noise are

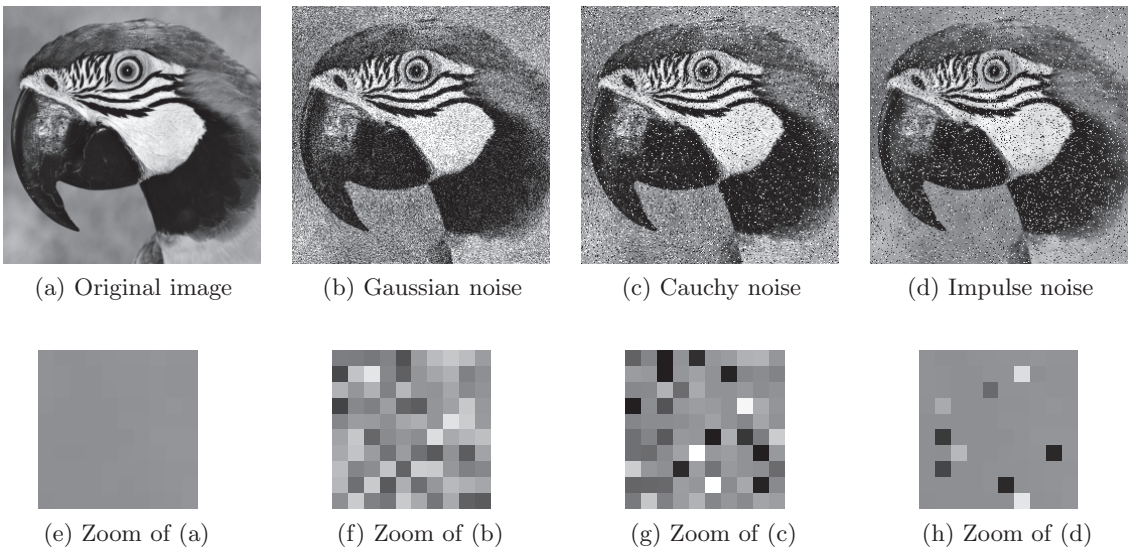

(a) Original image (b) Gaussian noise (c) Cauchy noise (d) Impulse noise

(e) Zoom of (a) (f) Zoom of (b) (g) Zoom of (c) (h) Zoom of (d)

Figure 3. *Comparison of different noisy images.* (a) *Original image* u_0*;* (b) u *corrupted by an additive Gaussian noise;* (c) u *corrupted by an additive Cauchy noise;* (d) u *corrupted by an impulse noise;* (e)–(h) *zooms of the top left corners of images* (a)–(d)*, respectively. The Cauchy noise and impulse noise are more impulsive than the Gaussian noise.*

quite close to each other. For instance, with the impulse noise and the Cauchy noisy there are some pixels degraded to white or black, while the image corrupted by the Gaussian noise is uniformly modified and white and black pixels are very rare. Although the Cauchy noise has some analogies with the impulse noise, there are also some very important differences; for example, in the impulse noise some pixels are noise-free (see Figure 3(h)), while in the Cauchy noise all the pixels are corrupted by noise (see Figure 3(g)). Thus, due to the impulsive character of the Cauchy noise and to its analogies with the impulse noise, we decide to employ the median filter in our minimization problem (4.1).

In the literature, there also exist some filters created for removing noise in impulsive environments, for instance the myriad filter [29, 30]. The myriad filter theory is based on the definition of the sample myriad as the maximum likelihood location estimator of the alpha-stable distribution. It is a very robust filter for suppressing impulsive noise, in particular alpha-stable noise, but comparing with the median filter it is much more sensitive with respect to the parameter selection and much more time-consuming. In section 5, we show the results obtained by applying the median filter and the myriad filter to the noisy images, and we can see that the myriad filter slightly outperforms the median filter. Furthermore, there is not any significant improvement if, in our model, we use the myriad filter instead of the median filter. Thus, for simplicity, we keep the median filter result as u_0 in our model (4.1).

4.2. Existence and uniqueness of a solution. We now prove that under certain conditions, there exists a unique solution for the minimization problem defined in (4.1). To do this, first of all we show that under certain conditions the objective function of (4.1) is strictly convex.

Proposition 4.1. *If* $8\mu\gamma^2 \geq 1$*, the model defined in* (4.1) *is strictly convex.*

Proof. We start to prove that the data fidelity term in (4.1) is strictly convex. Fixed $x \in \Omega$, we define a function $h : \mathbb{R} \to \mathbb{R}$ as

$$h(t) := \log\Big(\gamma^2 + \big(t - f(x)\big)^2\Big) + \mu\Big(t - u_0(x)\Big)^2, \tag{4.2}$$

and we prove that it is strictly convex. Easily, we can compute the first and the second order derivatives of h, and we have

$$h'(t) = 2\frac{t - f(x)}{\gamma^2 + (t - f(x))^2} + 2\mu(t - u_0(x)) \quad \text{and} \quad h''(t) = 2\frac{\gamma^2 - (t - f(x))^2}{\big(\gamma^2 + (t - f(x))^2\big)^2} + 2\mu.$$

A direct computation shows that h is strictly convex for $8\mu\gamma^2 \geq 1$. Since TV regularization is convex, we can also conclude that the objective function in (4.1) is strictly convex, for $8\mu\gamma^2 \geq 1$, and hence we have the thesis. ∎

We now prove the existence and uniqueness of a solution to (4.1).

Theorem 4.2. *Let f be in $L^\infty(\Omega)$; then the model (4.1) has a unique solution $u \in BV(\Omega)$ satisfying*

$$\min\left\{\inf_\Omega f, \inf_\Omega u_0\right\} \leq u \leq \max\left\{\sup_\Omega f, \sup_\Omega u_0\right\}.$$

Proof. The proof of the existence of a solution to (4.1) is similar to that for Theorem 3.1. We would like to mention that in this case the function defined in (4.2) is decreasing if $t < \min\{\inf f, \inf u_0\}$ and is increasing if $t > \max\{\sup f, \sup u_0\}$.

The uniqueness of the solution follows directly from the strict convexity of our model. ∎

As in section 3, we enunciate the minimum-maximum principle for the convex minimization problem. The proof of this proposition follows the same arguments as in Proposition 3.3.

Proposition 4.3. *Let f_1 and f_2 be in $L^\infty(\Omega)$ with $a_1 = \inf_\Omega f_1$ and $a_2 = \inf_\Omega f_2$, and we denote $b_1 = \sup_\Omega f_1$ and $b_2 = \sup_\Omega f_2$. Let us assume that $f_1 < f_2$. Then, denoting with u_1 (resp., u_2) a solution of (4.1) for $f = f_1$ (resp., $f = f_2$), we have $u_1 \leq u_2$ if $b_2 < a_1 + \gamma$.*

4.3. Deblurring and denoising case. We now modify our model to include a linear and continuous blurring operator $K \in \mathcal{L}(L^1(\Omega), L^2(\Omega))$. To restore a blurred image corrupted by Cauchy noise, we introduce the following optimization problem:

$$\inf_{u \in BV(\Omega)} \int_\Omega |Du| + \frac{\lambda}{2}\left(\int_\Omega \log\Big(\gamma^2 + (Ku - f)^2\Big)\mathrm{d}x + \mu\|Ku - u_0\|_2^2\right), \tag{4.3}$$

where u_0 is the image obtained by applying the median filter to the blurred and noisy image f.

Since the blurring operator K is nonnegative and it is linear, we can conclude that the model in (4.3) is convex when $8\mu\gamma^2 \geq 1$. In the following theorem we give the existence and uniqueness results to (4.3).

Theorem 4.4. *Let f be in $L^\infty(\Omega)$, let $u_0 \in L^2(\Omega)$, and let $K \in \mathcal{L}(L^1(\Omega), L^2(\Omega))$ be a nonnegative linear operator, and let assume that K does not annihilate constant functions, i.e., $KI \neq 0$. Then the model (4.3) admits a solution. If $8\mu\gamma^2 \geq 1$ and K is injective, there exists a unique solution.*

Proof. As in the proof of Theorem 3.1, one can prove that the objective function of the minimization problem in (4.3) is bounded from below. Consider a minimizing sequence

$\{u_n\} \in \mathrm{BV}(\Omega)$ for (4.3). From the boundedness of the objective function of our model, we have that $\{\int_\Omega |Du_n|\}$ is bounded. We define $m_\Omega(u_n) = \frac{1}{|\Omega|}\int_\Omega u_n dx$ with $|\Omega|$ as the measure of Ω. Based on the Poincaré inequality [23] we have

$$\|u_n - m_\Omega(u_n)\|_2 \leq C \int_\Omega |D(u_n - m_\Omega(u_n))| = C \int_\Omega |Du_n|,$$

where C is a positive constant. Recalling that Ω is bounded, we have that $\|u_n - m_\Omega(u_n)\|_2$ and $\|u_n - m_\Omega(u_n)\|_1$ are bounded for each n. Due to the continuity of the blurring operator $K \in \mathcal{L}(L^1(\Omega), L^2(\Omega))$, the sequence $\{K(u_n - m_\Omega(u_n))\}$ is bounded in $L^2(\Omega)$ and in $L^1(\Omega)$. Furthermore, since the objective function of (4.3) is bounded, we also have that $(Ku_n - u_0)^2$ is bounded in $L^1(\Omega)$ for each n; thus $\|Ku_n - u_0\|_1$ is bounded and hence $\|Ku_n\|_1$ is bounded. We are now ready to prove that $|m_\Omega(u_n)|\|KI\|_1$ is bounded from

$$|m_\Omega(u_n)|\|KI\|_1 = \|K(u_n - m_\Omega(u_n)) - Ku_n\|_1 \leq \|K(u_n - m_\Omega)\|_1 + \|Ku_n\|_1.$$

Since $KI \neq 0$, we have that $m_\Omega(u_n)$ is uniformly bounded. Thus, now we can conclude that the sequence $\{u_n\}$ is bounded in $L^2(\Omega)$ and hence in $L^1(\Omega)$. Thus, since $BV(\Omega)$ is closed and convex, $\{u_n\}$ is also bounded in $BV(\Omega)$. Thus, there exists a subsequence $\{u_{n_k}\}$ which converges strongly in $L^1(\Omega)$ to some $u^\star \in BV(\Omega)$, and $\{Du_{n_k}\}$ converges weakly as a measure to $Du^\star$. Since K is a continuous linear operator, $\{Ku_{n_k}\}$ converges strongly to $Ku^\star$ in $L^2(\Omega)$. Moreover, up to a subsequence, $\{Ku_{n_k}\}$ converges almost everywhere to this $Ku^\star$. Based on the lower semicontinuity of TV and Fatou's lemma, we have that $u^\star$ is a solution of (4.3).

The uniqueness of the solution follows directly from the injectivity of the operator K and the assumption of $8\mu\gamma^2 \geq 1$, since in this case the model is strictly convex. ■

Note that the assumption that $K \in \mathcal{L}(L^1(\Omega), L^2(\Omega))$ is classical; see [15]. Basically, the above proof also works when $K =$Id. We leave the details to the interested reader.

4.4. Numerical method. In this part we show how to compute numerically the minimizer of (4.3). We focus directly on the general case, since the denoising case can be seen as a special case of the deblurring and denoising one, when K is the identity operator. First of all, we derive the discrete version of our minimization problem (4.3), and then we study how to solve it numerically. For the sake of simplicity we keep the notation from the continuous contest. Let $f \in \mathbb{R}^{mn}$ be the noisy image obtained from a two-dimensional pixel-array, with dimension $m \times n$, by concatenation in the usual columnwise fashion, and let $K \in \mathbb{R}^{mn \times mn}$ be the discretization of the continuous blurring operator K. Due to the convexity of (4.3), there exist many algorithms to solve the proposed model, for instance the primal dual algorithm [10, 14, 17], the alternating direction method with multipliers (ADMM) [6], the split-Bregman algorithm [28], and the Chambolle–Pock algorithm [11]. Since, under some hypothesis, the convergence of the Chambolle–Pock algorithm is guaranteed (see [11]), we decide to employ it to solve our minimization problem (3.8).

In order to compute numerically the solution of our minimization problem, we introduce the discrete version of (4.3),

$$\min_u \|\nabla u\|_1 + \frac{\lambda}{2} G(Ku), \tag{4.4}$$

where $G : \mathbb{R}^{mn} \to \mathbb{R}$ represents the data fidelity term and it is defined as follows:

$$G(u) := \sum_i \log\left(\gamma^2 + (u_i - f_i)^2\right) + \mu\|u - u_0\|_2^2.$$

The first term of (4.4) represents the discrete TV of the image u, and it is defined as follows:

$$\|\nabla u\|_1 = \sum_i \sqrt{(\nabla_x u)_i^2 + (\nabla_y u)_i^2}.$$

The discrete gradient $\nabla \in \mathbb{R}^{2mn \times mn}$ is given by

$$\nabla u = \begin{pmatrix} \nabla_x u \\ \nabla_y u \end{pmatrix},$$

where the discrete derivative operators in the x-direction and y-direction, respectively, ∇_x and ∇_y, are obtained using the finite difference approximations to the derivatives with symmetric boundary conditions,

$$(\nabla_x u)_{l,j} = \begin{cases} u_{l+1,j} - u_{l,j} & \text{if } l < n, \\ 0 & \text{if } l = n \end{cases} \quad \text{and} \quad (\nabla_y u)_{l,j} = \begin{cases} u_{l,j+1} - u_{l,j} & \text{if } j < m, \\ 0 & \text{if } j = m. \end{cases}$$

As in [13], for using the primal dual algorithm, we introduce two new variables $v \in \mathbb{R}^{2mn}$ and $w \in \mathbb{R}^{mn}$, and, instead of consider the unconstrained problem, we look at the following constrained optimization problem:

$$\min_{u,v,w} \|v\|_1 + \frac{\lambda}{2} G(w) \text{ subject to } v = (v_x, v_y)^\top = \nabla u \text{ and } w = Ku. \tag{4.5}$$

To apply the Chambolle–Pock algorithm, we study the following optimization problem:

$$\min_{u,v,w \in \mathbb{R}^{mn}} \max_{p,q \in Y} \|v\|_1 + \frac{\lambda}{2} G(w) + \langle v - \nabla u, p\rangle + \langle w - Ku, q\rangle, \tag{4.6}$$

where $p \in \mathbb{R}^{2mn}$ and $q \in \mathbb{R}^{mn}$ are the dual variables, and $Y = \{q \in \mathbb{R}^{2mn} : \|q\|_\infty \le 1\}$, where $\|q\|_\infty$ is the ℓ^∞-vector norm and it is defined as follows:

$$\|q\|_\infty = \max_{i \in \{1,\dots,mn\}} \sqrt{q_i^2 + q_{i+mn}^2}.$$

Then the Chambolle–Pock algorithm for solving (4.6) is described in Algorithm 1. The main calculation is carried out in (4.7)–(4.11). In the following, we give the details on how to solve them.

Algorithm 1. Solving (4.6) by using the Chambolle–Pock algorithm.

1: Fixed $\sigma > 0$ and $\tau > 0$. Initialize: $p^0 = 0$, $q^0 = 0$, $u^0 = \bar{u}^0 = f$, $v^0 = \bar{v}^0 = \nabla u^0$, and $w^0 = \bar{w}^0 = Ku^0$.

2: Calculate p^{k+1}, q^{k+1}, u^{k+1}, v^{k+1}, w^{k+1}, $\bar{u}^{k+1}$, $\bar{v}^{k+1}$, and $\bar{v}^{k+1}$ using the following equations:

$$p^{k+1} = \arg\max_p \langle \bar{v}^k - \nabla \bar{u}^k, p\rangle - \frac{1}{2\sigma}\|p - p^k\|_2^2, \tag{4.7}$$

$$q^{k+1} = \arg\min_q \langle \bar{w}^k - K\bar{u}^k, q\rangle - \frac{1}{2\sigma}\|q - q^k\|_2^2, \tag{4.8}$$

$$u^{k+1} = \arg\min_u -\langle \nabla u, p^{k+1}\rangle - \langle Ku, q^{k+1}\rangle + \frac{1}{2\tau}\|u - u^k\|_2^2, \tag{4.9}$$

$$v^{k+1} = \arg\min_v \|v\|_1 + \langle v, p^{k+1}\rangle + \frac{1}{2\tau}\|v - v^k\|_2^2, \tag{4.10}$$

$$w^{k+1} = \arg\min_w \frac{\lambda}{2}G(w) + \langle w, q^{k+1}\rangle + \frac{1}{2\tau}\|w - w^k\|_2^2, \tag{4.11}$$

$$\bar{u}^{k+1} = 2u^{k+1} - u^k, \tag{4.12}$$

$$\bar{v}^{k+1} = 2v^{k+1} - v^k, \tag{4.13}$$

$$\bar{w}^{k+1} = 2w^{k+1} - w^k. \tag{4.14}$$

3: Stop or set $k := k + 1$ and go back to step 2.

The objective functions (4.7)–(4.9) are quadratics, and thus the update of p, q, and u is given by

$$\begin{aligned} p^{k+1} &= \sigma(\bar{v}^k - \nabla \bar{u}^k) + p^k, \\ q^{k+1} &= \sigma(\bar{w}^k - K\bar{u}^k) + q^k, \\ u^{k+1} &= u^k + \tau(K^\top q^{k+1} - \mathrm{div} p^{k+1}). \end{aligned} \tag{4.15}$$

The equation in (4.10) can be rewritten in the following way:

$$v^{k+1} = \arg\min_v \|v\|_1 + \frac{1}{2\tau}\|v - t^k\|_2^2,$$

where $t^k = v^k - \tau p^{k+1}$. Thus, the update of v is easily given by applying the soft shrinkage operator,

$$v_i^{k+1} = \frac{t_i^k}{|t_i^k|}\max\{|t_i^k| - \tau, 0\} \text{ and } v_{i+mn}^{k+1} = \frac{t_{i+mn}^k}{|t_i^k|}\max\{|t_i^k| - \tau, 0\} \text{ for } i = 1, \ldots, mn,$$

with $|t_i^k| = \sqrt{(t_i^k)^2 + (t_{i+mn}^k)^2}$.

The optimality condition for (4.11) is given by

$$\lambda\frac{w - f}{\gamma^2 + (w - f)^2} + \mu\lambda(w - u_0) + q^{k+1} + \frac{1}{\tau}(w - w^k) = 0, \tag{4.16}$$

where, as usual, the division and the exponentiation have to be considered pointwise.

Multiplying both sides of the above equation for $\tau(\gamma^2+(w-f)^2)$, collecting the term with the same factors, one can see that (4.16) is equivalent to the following cubic equation:

$$aw^3+bw^2+cw+d=0,$$

with

$$\begin{aligned}
a &= \mu\lambda\tau+1;\\
b &= -(\mu\lambda\tau(2f+u_0)-\tau q^{k+1}+2f+w^k);\\
c &= \tau\lambda+\mu\lambda\tau(\gamma^2+f^2+2u_0f)-2\tau q^{k+1}f+\gamma^2+f^2+2w^kf;\\
d &= -\tau\lambda f-\mu\lambda\tau u_0(\gamma^2+f^2)+\tau q^{k+1}(\gamma^2+f^2)-w^k(\gamma^2+f^2).
\end{aligned}$$

From Cardano's formula, we can find the explicit expression for the solutions of a cubic equation; see the following proposition. For more details, we refer the reader to [37].

Proposition 4.5. *A generic cubic equation with real coefficients*

$$ax^3+bx^2+cx+d=0, \text{ with } a\neq 0, \tag{4.17}$$

has at least one solution among the real numbers. Let

$$q=\frac{3ac-b^2}{9a^2} \quad \text{and} \quad r=\frac{9abc-27a^2d-2b^3}{54a^3};$$

if there exists a unique real solution of (4.17), the discriminant, $\Delta=q^3+r^2$, has to be positive. Furthermore, if $\Delta\geq 0$, the only real root of (4.17) is given by

$$x=\sqrt[3]{r+\sqrt{\Delta}}+\sqrt[3]{r-\sqrt{\Delta}}-\frac{b}{3a}. \tag{4.18}$$

Due to the strict convexity of our problem, we know that there exists a unique real solution for (4.16) and, from the above proposition, it can be computed explicitly using (4.18). Otherwise, since the objective function in (4.11) has the second derivative, one can also determine the solution in an efficient way using the Newton method followed by one projection step, in order to guarantee the nonnegativity of u; see [21, 34]. In our simulations, we decide to compute the explicit expression of unique real solution by using Cardano's formula.

We remark that if K is the identity operator, i.e., the degraded image f is not blurred but it is only corrupted by noise, there is no need to introduce the primal variable w and the dual variable q, and the algorithm can be simplified accordingly.

In the last part of this section, we study the existence of the solution and the convergence of the algorithm. First of all, we reformulate (4.6) in the following way:

$$\min_x \max_y \; H(x)+\langle Ax,y\rangle, \tag{4.19}$$

with $H(x)=\|v\|_1+\frac{\lambda}{2}G(w)$ and

$$A=\begin{pmatrix}-\nabla & I & 0\\ -K & 0 & I\end{pmatrix}, \quad x=\begin{pmatrix}u\\ v\\ w\end{pmatrix}, \quad \bar{x}=\begin{pmatrix}\bar{u}\\ \bar{v}\\ \bar{w}\end{pmatrix}, \quad y=\begin{pmatrix}p\\ q\end{pmatrix}.$$

Proposition 4.6. *The saddle-point set of* (4.19) *is nonempty.*

For the proof, we refer the reader to Proposition 2 in [44].

The following proposition shows the convergence of the algorithm described in Algorithm 1.

Proposition 4.7. *The iterates* (x^k, y^k) *defined in Algorithm 1 converge to a saddle point of the primal dual problem defined in* (4.19) *if* $\sigma\tau\|A\|_2^2 < 1$, *where* $\|A\|_2$ *denotes the operator* 2*-norm of* A.

This proposition can be seen as a special case of the theorem proved by Chambolle and Pock [11, Theorem 1].

In order to use the inequality given in the above proposition, we need to give an estimate of $\|A\|_2$. By using the property of the norm, one can find that

$$\|Ax\|_2 \leq \sqrt{\|\nabla\|_2^2 + \|K\|_2^2}\|u\|_2 + \left\|\begin{pmatrix} v \\ w \end{pmatrix}\right\|_2.$$

If $\|x\|_2 = 1$, by definition of x, we have that $\|u\|_2^2 + \left\|\binom{v}{w}\right\|_2^2 = 1$; therefore, from the Cauchy inequality, we obtain

$$\|Ax\|_2 \leq \sqrt{\|\nabla\|_2^2 + \|K\|_2^2 + 1}.$$

Hence, we have $\|A\|_2 \leq \sqrt{\|\nabla\|_2^2 + \|K\|_2^2 + 1}$.

From [10], we know that $\|\nabla\|_2^2 \leq 8$, and from [44], we have that $\|K\|_2 \leq 1$, and thus $\|A\|_2 \leq \sqrt{10}$. Therefore, in order to ensure the convergence of our algorithm we just need that $\sigma\tau < 0.1$. In our numerical simulations we set $\sigma = \tau = 0.3$, which ensures the convergence of the algorithm.

5. Numerical simulations.

In this section, we show some numerical reconstructions obtained by applying our proposed model to blurred images corrupted by Cauchy noise. First of all, we focus only on the denoising case, and then we consider also the deblurring case. In order to show the potentiality of our method, we compare our reconstructions with images obtained by employing other well-known methods, such as the ROF model [54], the median filter [25], the myriad filter [29], and the L^1-TV model. The L^1-TV model was introduced by Nikolova in [45, 46] for restoring images corrupted by impulse noise; in particular, in this model, the TV regularization is combined with an L^1 data fidelity term. Motivated by the impulsive character of the Cauchy noise, we decide to compare our reconstructions also with the L^1-TV model. For the ROF model and the L^1-TV model, we employ the primal dual algorithm proposed in [11] to solve the minimization problem. Furthermore, in Figure 9, we also compare our method with other methods, such as the wavelet shrinkage [5], the SURE-LET [43], and the BM3D [18].

For illustrations, we use the 256-by-256 gray level images Peppers, Parrot, and Cameraman; the original images are presented in Figure 4. The quality of the restored images is compared quantitatively using the peak signal noise ratio (PSNR) value [5] and the measure of structural similarity (SSIM) [64]. The PSNR is a measure widely used in image quality assessment, and it is defined as follows:

$$\mathrm{PSNR} = 20\log_{10}\frac{mn|u_{\max} - u_{\min}|}{\|u^\star - u\|_2},$$

(a) (b) (c)

Figure 4. *Original images.* (a) *Peppers;* (b) *Parrot;* (c) *Cameraman.*

where $u^\star$ and u are, respectively, the restored and the original images with values in the gray-level range $[u_{\min}, u_{\max}]$. It is a very useful tool, since it is able to measure quantitatively the quality of the reconstructed image compared to the original image. Recently, another measure has become very popular in the imaging community, the so-called SSIM measure. This measure compares local patterns of pixel intensities that have been normalized for luminance and contrast, and it has been proved that it is more consistent with human eye perception than PSNR [64].

In our simulations, we stop our algorithm as soon as there are not big changes in the objective function, i.e.,

$$\frac{E(u^k) - E(u^{k-1})}{E(u^k)} < 5 \cdot 10^{-5},$$

where E denotes the objective function of the proposed minimization problem. In our method, we choose the regularization parameter λ to give a good balance between a good fit to f and the smoothness from TV. Since γ depends on the noise level, we use the same value of γ for all test images under the same noise level. Based on our numerical experiments, our method is robust with respect to μ; so we choose it such that the convexity condition is just satisfied, i.e., $8\mu\gamma^2 = 1$. The development of an automatic procedure for choosing these parameters is outside the scope of this paper. In addition, all the simulations are run in MATLAB R2014a.

5.1. Image denoising. In this section we focus only on the denoising case. Our aim is to recover the original image u, knowing the corrupted image f. Since the ratio of two independent standard normal variables gives a standard Cauchy random variable, we generate the noisy image f by using the following equation:

$$f = u + v = u + \xi \frac{\eta_1}{\eta_2},$$

where the random variable v follows the Cauchy distribution, $\xi > 0$ gives the noise level, and η_1 and η_2 follow the Gaussian distribution with mean 0 and variance 1.

In the following, we compare our reconstructions with those obtained by applying the ROF model, the median filter (MD), the myriad filter (MR), and the L^1-TV model. By tuning the regularization parameter λ, in the ROF model and the L^1-TV model, we use the results with the best PSNRs to compare with our method.

In Figures 5 and 7, we give the results for denoising the corrupted images Peppers, Parrot, and Cameraman for different noise levels, $\xi = 0.02$ and $\xi = 0.04$. In order to make evident

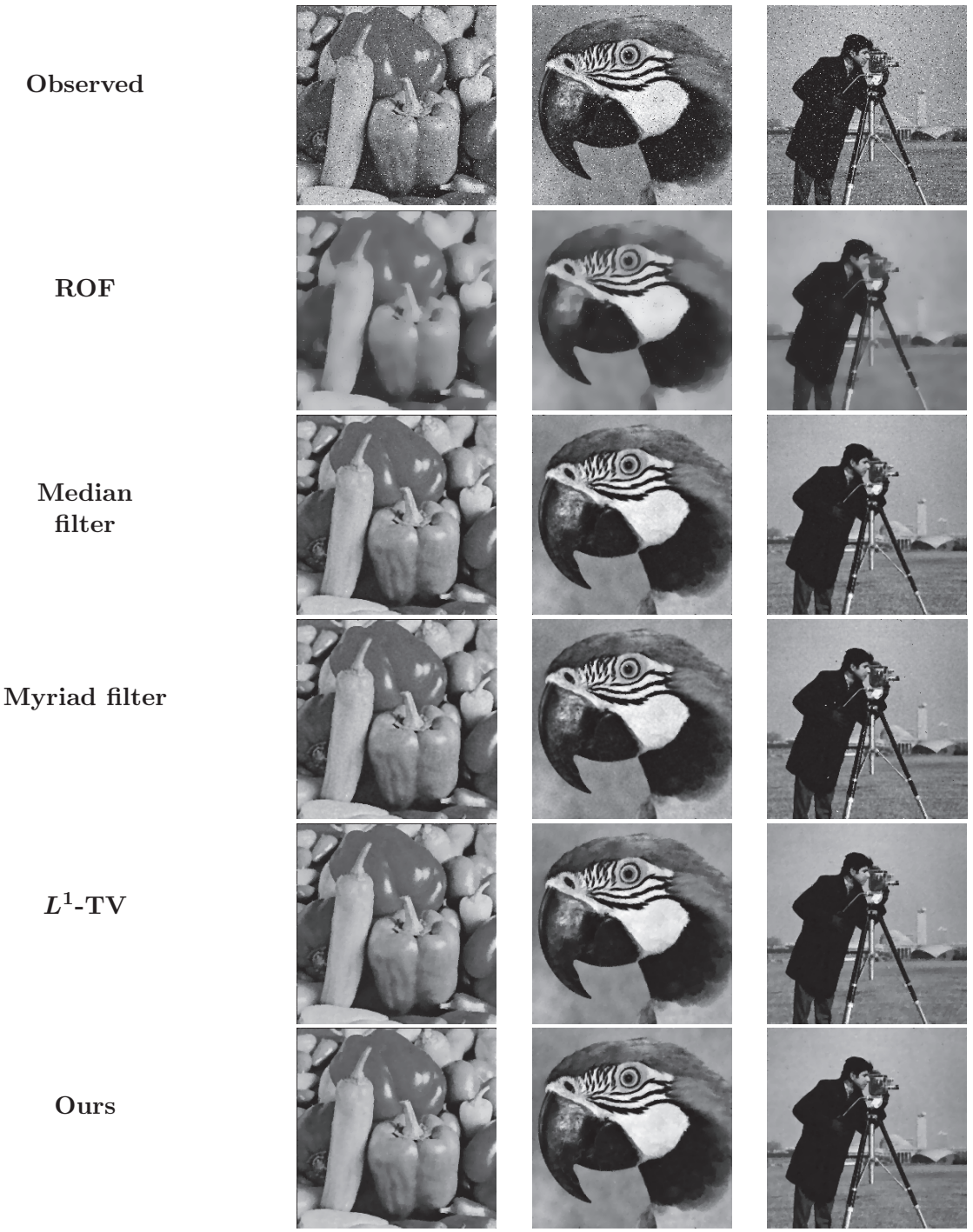

Figure 5. *Comparison of the recovered images from different methods for removing Cauchy noise in Peppers ("Pe" for short), Parrot ("Pa"), and Cameraman ("C"). First row: noisy images f ($\xi = 0.02$); second row: restored images by the ROF approach ($\lambda = 5$ ("Pe"); 6 ("Pa"); 5.8 ("C")); third row: restored images by the median filter (MD); fourth row: restored images by the myriad filter (MR); fifth row: restored images by the L^1-TV approach ($\lambda = 1.5$ ("Pe"); 1.5 ("Pa"); 1.6 ("C")); sixth row: restored images by our approach ($\lambda = 0.7$ ("Pe"); 0.8 ("Pa"); 0.7 ("C"), $\mu = 6.25$, and $\gamma = \frac{\sqrt{2}}{10}$).*

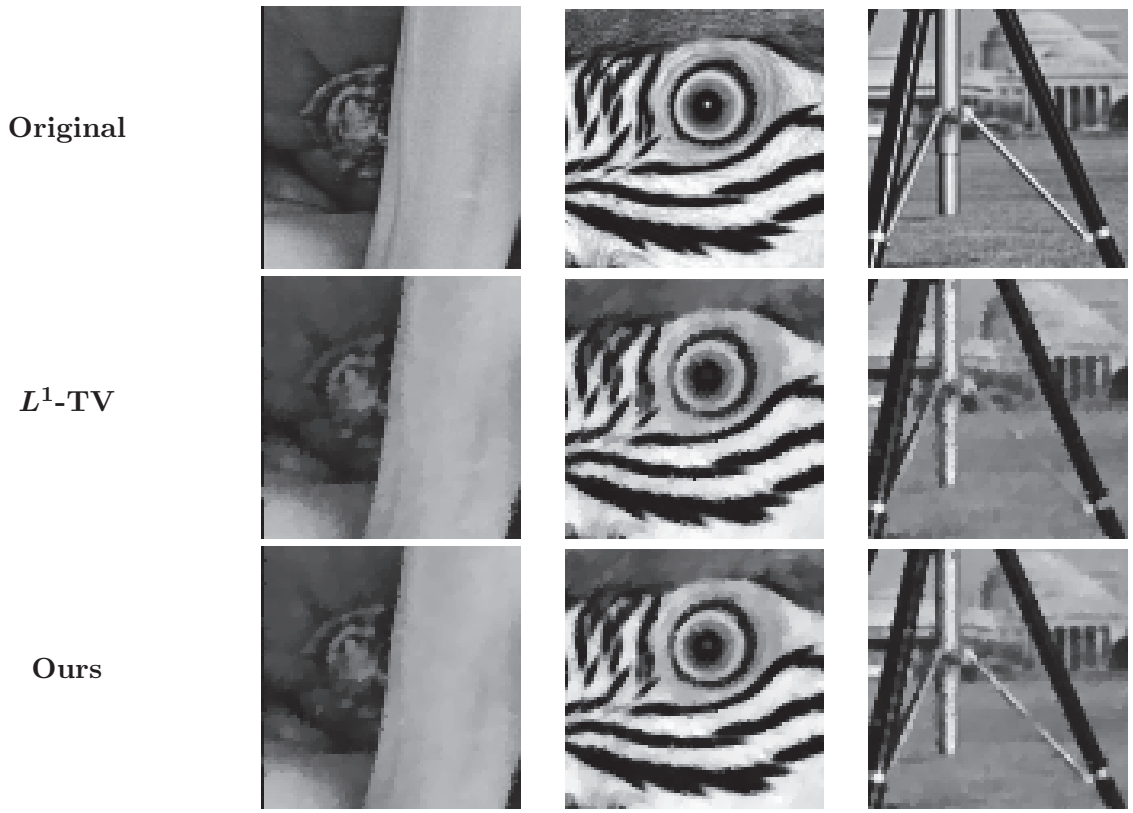

Figure 6. *The zoomed-in regions of the recovered images in Figure 5. First row: details of original images; second row: details of restored images by the L^1-TV approach; third row: details of restored images by our approach.*

the differences between the L^1-TV approach and ours, in Figure 6 we present some details of Figure 5 (here, we also include the original images in the first row). It can be seen that the L^1-TV model outperforms the ROF model, the median filter, and the myriad filter, but our method gives even better visual quality. The reason why our method and the L^1-TV approach perform better is because Cauchy noise is very impulsive and in some way it is very similar to impulse noise; see subsection 4.1. Since the ROF model was introduced for removing Gaussian noise, in order to remove highly impulsive Cauchy noise, it has to oversmooth the image. For example, in Cameraman many details are missing and the contrast of the image is reduced. The median filter and the myriad filter work quite well if the noise level is low; otherwise they are not able to eliminate all the noise and at the same time to preserve most details. From the details in Figure 6, we can see that our reconstructions preserve better the details of the image, for example the stalk of the Peppers, the eye and the stripes of the Parrot, and the tripod and the column of the building in Cameraman.

For the comparison of the performance quantitatively, in Tables 1–4 we list the values of the PSNR and SSIM for the noisy and recovered images. Here, we also provide the values of PSNR and SSIM for other popular test images in image processing, such as Lena, Baboon,

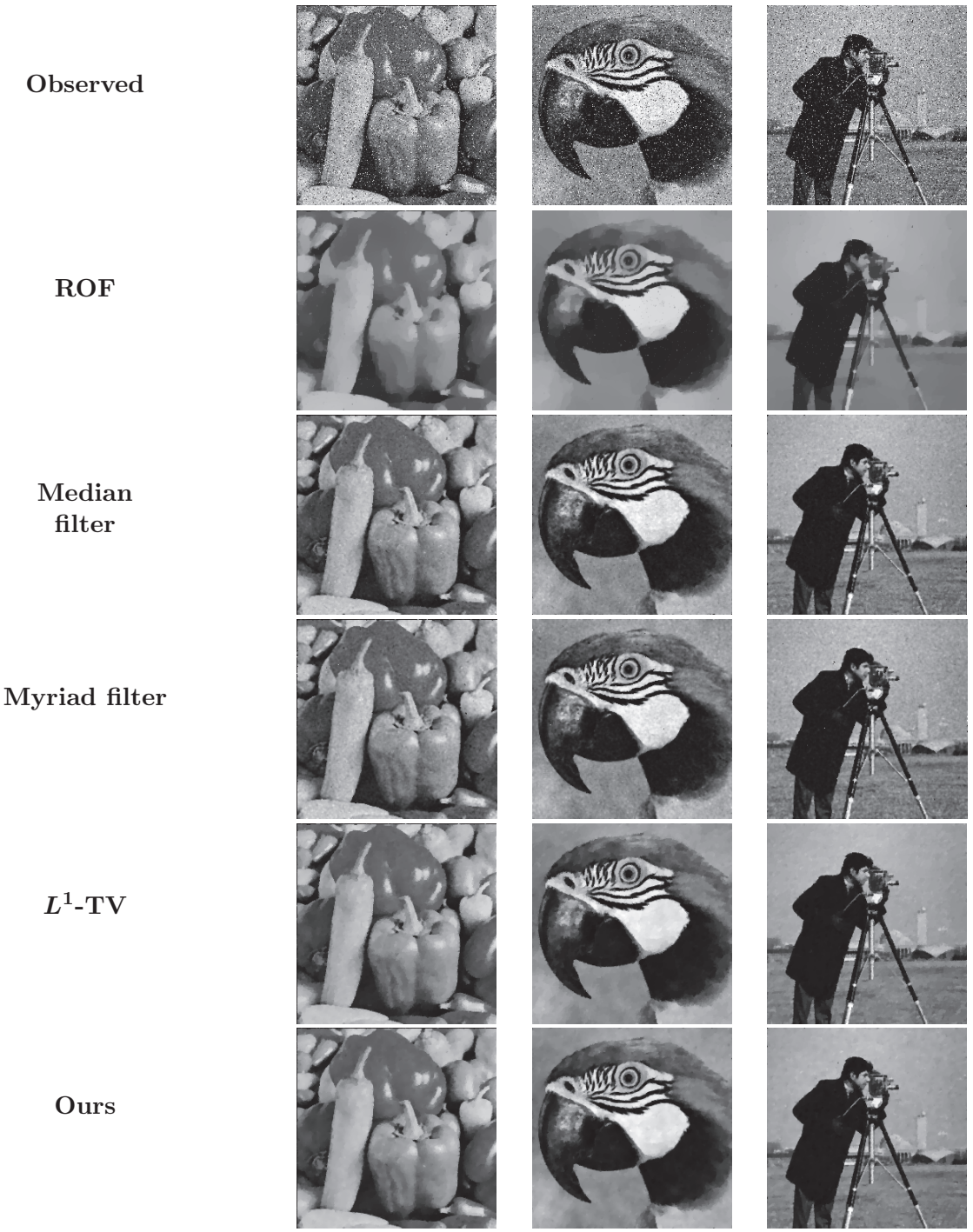

Figure 7. *Comparison of the recovered images from different methods for removing Cauchy noise. First row: noisy images f ($\xi = 0.04$); second row: restored images by the ROF approach ($\lambda = 4.5$ ("Pe"); 4.7 ("Pa"); 5 ("C")); third row: restored images by the median filter (MD); fourth row: restored images by the myriad filter (MR); fifth row: restored images by the L^1-TV approach ($\lambda = 1.3$ ("Pe"); 1.3 ("Pa"); 1.5 ("C")); sixth row: restored images by our approach ($\lambda = 0.6$ ("Pe"); 0.8 ("Pa"); 0.9 ("C"), $\mu = 3.125$, and $\gamma = 0.2$).*

Table 1

PSNR values for noisy images and recovered images given by different methods ($\xi = 0.02$). In the last line of the table, we compute the average of the values.

	Noisy	ROF	MD	MR	L^1-TV	**Ours**
Peppers	19.15	25.03	29.64	29.85	30.34	**30.94**
Parrot	19.13	23.88	27.05	27.13	28.02	**28.98**
Cameraman	19.07	24.00	26.14	26.57	27.21	**27.91**
Lena	19.06	24.58	28.94	28.98	29.84	**30.36**
Baboon	19.17	21.16	21.38	21.64	24.24	**24.96**
Goldhill	18.99	24.40	26.80	27.12	28.23	**28.80**
Boat	19.03	24.21	27.27	27.49	28.70	**29.20**
Average	19.09	23.89	26.75	26.97	28.08	**28.74**

Table 2

SSIM measures for noisy images and recovered images given by different methods ($\xi = 0.02$). In the last line of the table, we compute the average of the values.

	Noisy	ROF	MD	MR	L^1-TV	**Ours**
Peppers	0.3243	0.4820	0.6743	0.6790	0.7163	**0.7168**
Parrot	0.3179	0.4083	0.5894	0.5697	0.6571	**0.6641**
Cameraman	0.2743	0.2314	0.4115	0.4180	0.4715	**0.4707**
Lena	0.3240	0.4022	0.6488	0.6370	0.6950	**0.6880**
Baboon	0.5174	0.2115	0.4231	0.4175	0.6980	**0.6950**
Goldhill	0.3744	0.3191	0.5875	0.5952	0.6692	**0.6811**
Boat	0.3566	0.3474	0.6437	0.6387	0.6908	**0.6931**
Average	0.3556	0.3431	0.5683	0.5650	0.6568	**0.6584**

Table 3

PSNR values for noisy images and recovered images given by different methods ($\xi = 0.04$). In the last line of the table, we compute the average of the values.

	Noisy	ROF	MD	MR	L^1-TV	**Ours**
Peppers	16.25	23.95	27.25	27.50	28.29	**28.80**
Parrot	16.27	22.75	25.50	25.85	26.55	**27.16**
Cameraman	16.08	23.17	24.87	25.19	25.99	**26.66**
Lena	16.21	24.29	26.88	27.03	28.79	**29.30**
Baboon	16.16	20.67	20.90	21.55	22.50	**23.05**
Goldhill	16.21	23.72	25.48	25.85	26.49	**27.00**
Boat	16.28	23.55	25.67	25.16	26.67	**27.18**
Average	16.21	23.16	25.22	25.45	26.47	**27.02**

Goldhill, and Boat. From Tables 1–4, we can see that, on average, with our method we can increase the PSNRs of the recovered images of 0.66 dB for $\xi = 0.02$ and 0.55 dB for $\xi = 0.04$

Table 4

SSIM measures for noisy images and recovered images given by different methods ($\xi = 0.04$). In the last line of the table, we compute the average of the values.

	Noisy	ROF	MD	MR	L^1-TV	**Ours**
Peppers	0.2246	0.4294	0.5605	0.5734	0.6347	**0.6411**
Parrot	0.2334	0.3289	0.4706	0.4800	0.5529	**0.5676**
Cameraman	0.1989	0.2081	0.3379	0.3452	0.3857	**0.3920**
Lena	0.2220	0.4025	0.5394	0.5500	0.5993	**0.6170**
Baboon	0.3651	0.1588	0.3681	0.3795	0.5525	**0.5650**
Goldhill	0.2426	0.2786	0.5108	0.5256	0.5205	**0.5684**
Boat	0.2479	0.3266	0.5429	0.5498	0.5843	**0.5930**
Average	0.2478	0.3047	0.4757	0.4862	0.5471	**0.5634**

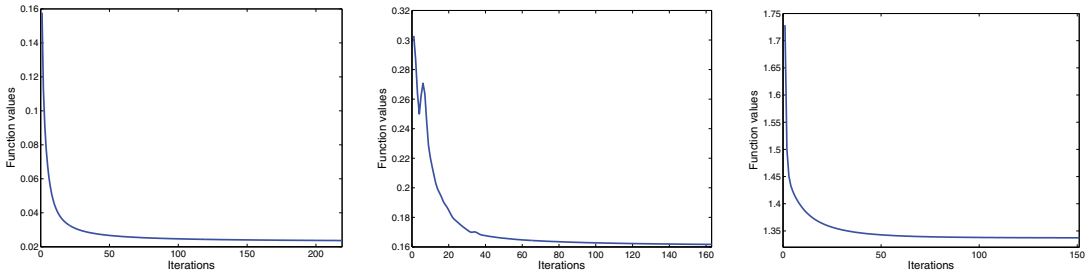

(a) (b) (c)

Figure 8. *Plots of the objective function values versus iterations of the three TV-based methods corresponding to the experiments in the first line of Figure 5.* (a) *ROF model;* (b) *L^1-TV model;* (c) *our model.*

and also obtain largest SSIM values.

The convergence of the algorithm of the three TV-based methods is presented in Figure 8, where we plot the objective function values versus the number of iterations (we use the image of the Parrot when $\xi = 0.02$). Here, we see that the objective function values for the ROF model and ours are monotonically decreasing.

Finally, we compare our method with some well-known techniques in image denoising. Here, we use the noisy image Peppers with PSNR=19.15 and we compare with the wavelet shrinkage [5], the SURE-LET [43], and the BM3D [18]. From Figure 9, we can clearly see that our method outperforms all of them. Visually, there is still some noise left in the results from the other three methods, which is due to the impulsive behavior of Cauchy noise.

5.2. Image deblurring and denoising. In this section, we consider restoring blurred images corrupted by Cauchy noise. In our simulation, we use the Gaussian blur with a window size 9×9 and standard deviation of 1. After the blurring operation, we corrupt the images by adding Cauchy noise with $\xi = 0.02$. As in the previous section we compare our reconstructions with those obtained by employing the ROF model, the median filter, the myriad filter, and the L^1-TV model; see Figures 10 and 11. In Tables 5 and 6, we list the values of the PSNR and SSIM for different images and different variational methods.

(a) Wavelet: 23.13 (b) SURE-LET: 23.22 (c) BM3D: 28.74 (d) Ours: 30.94

Figure 9. *Recovered images (with PSNR(dB)) of different approaches for removing Cauchy noise using as the noisy image that in the first column of Figure 5.* (a) *Wavelet shrinkage;* (b) *SURE-LET;* (c) *BM3D;* (d) *our model.*

Comparing the results of the three TV-based methods, i.e., the ROF, the L^1-TV, and ours, one can see that our method performs best visually. The images given by the ROF model are too smooth, and the details are missed. The L^1-TV model preserves more details than the ROF model, but still some features are lost or not well recovered as in our model, such as the eye of the Parrot and the columns of the building in the Cameramen; see Figure 11. In the third and fourth rows of Figure 10, the reconstructions given by the median filter and the myriad filter are shown. We can see that the images are still blurred, because there are no deblurring steps in both filters. Comparing the values of the PSNR and SSIM, we can clearly see that our method outperforms the others even in presence of blur.

6. Conclusion.

In this paper, we introduce a variational method for deblurring and denoising of blurred images corrupted by Cauchy noise. Inspired by the ROF model we combine a TV regularization term with a data fidelity term suitable for the Cauchy noise. In order to obtain a convex minimization problem, we add a quadratic penalty term based on the median filter. Due to the strict convexity of our problem, we are able to prove the existence and the uniqueness of a solution to our proposed model. Then, we introduce the primal dual algorithm to solve our convex minimization problem and the convergence is ensured. Numerical results show that our method outperforms other existing and well-known methods.

Appendix. Proof of Proposition 3.3.

In this section we give more details on the proof of Proposition 3.3; in particular we show that the integrand of (3.7) is strictly negative.

Using the properties of the logarithm, we can rewrite the last inequality in the proof as follows:

$$\int_{\{u_1>u_2\}} \log \frac{(\gamma^2+(u_2-f_1)^2)(\gamma^2+(u_1-f_2)^2)}{(\gamma^2+(u_1-f_1)^2)(\gamma^2+(u_2-f_2)^2)}\mathrm{d}x \geq 0. \tag{A.1}$$

Now we show that, under our assumptions, the integrand of (A.1) is strictly negative. Since the argument of the logarithm in (A.1) is strictly positive, we just need to show that

$$\frac{(\gamma^2+(u_2-f_1)^2)(\gamma^2+(u_1-f_2)^2)}{(\gamma^2+(u_1-f_1)^2)(\gamma^2+(u_2-f_2)^2)} < 1. \tag{A.2}$$

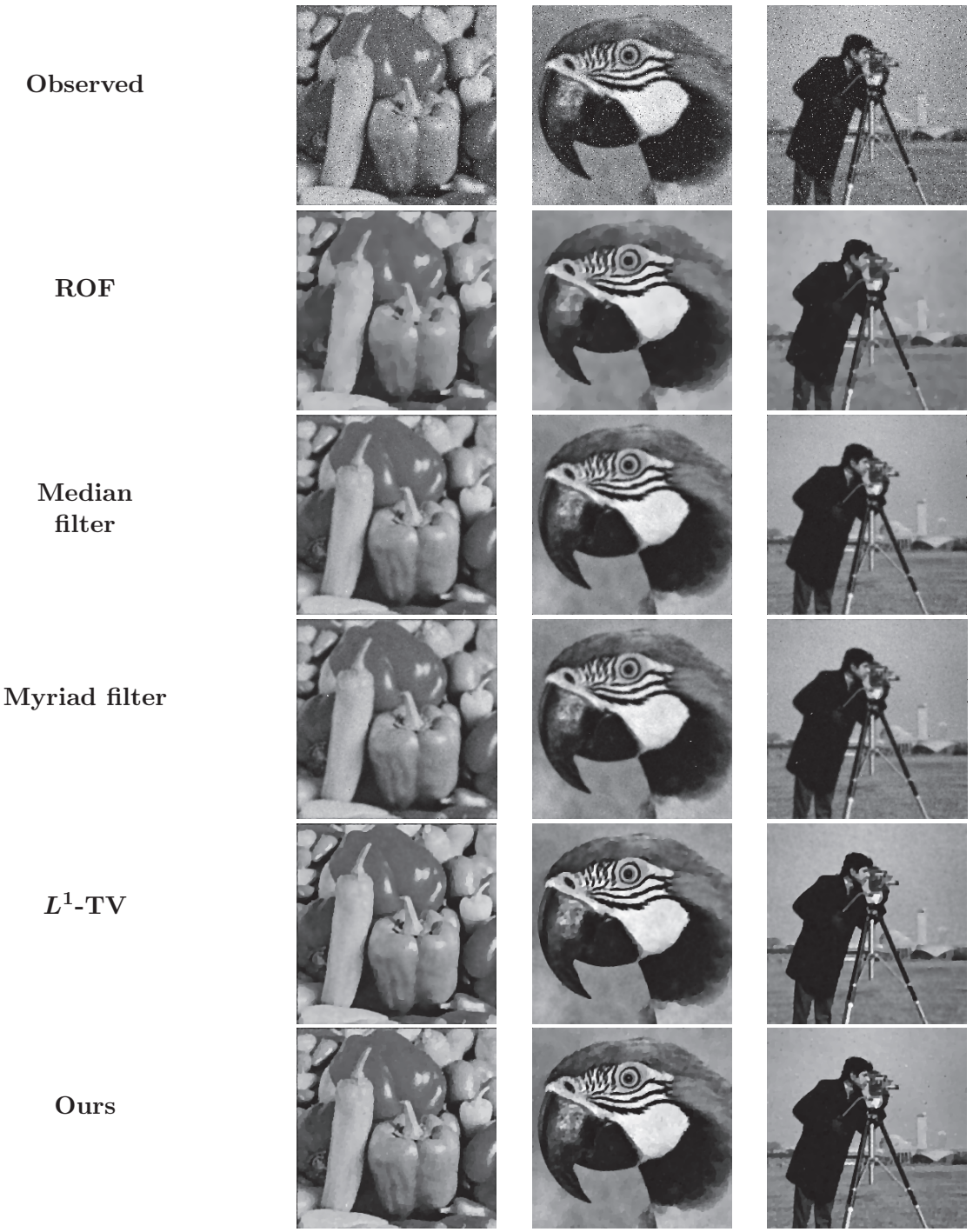

Figure 10. *Comparison of the recovered images from different methods for deblurring and denoising an image blurred and corrupted by Cauchy noise. First row: blurred and noisy images f ($\xi = 0.02$); second row: restored images by the ROF approach ($\lambda = 15$ ("Pe"); 16 ("Pa"); 16 ("C")); third row: restored images by the median filter (MD); fourth row: restored images by the myriad filter (MR); fifth row: restored images by the L^1-TV approach ($\lambda = 3$ ("Pe"); 3.4 ("Pa"); 3.5 ("C")); sixth row: restored images by our approach ($\lambda = 2$ ("Pe"); 2.1 ("Pa"); 2.1 ("C"), $\mu = 6.25$, and $\gamma = \frac{\sqrt{2}}{10}$).*

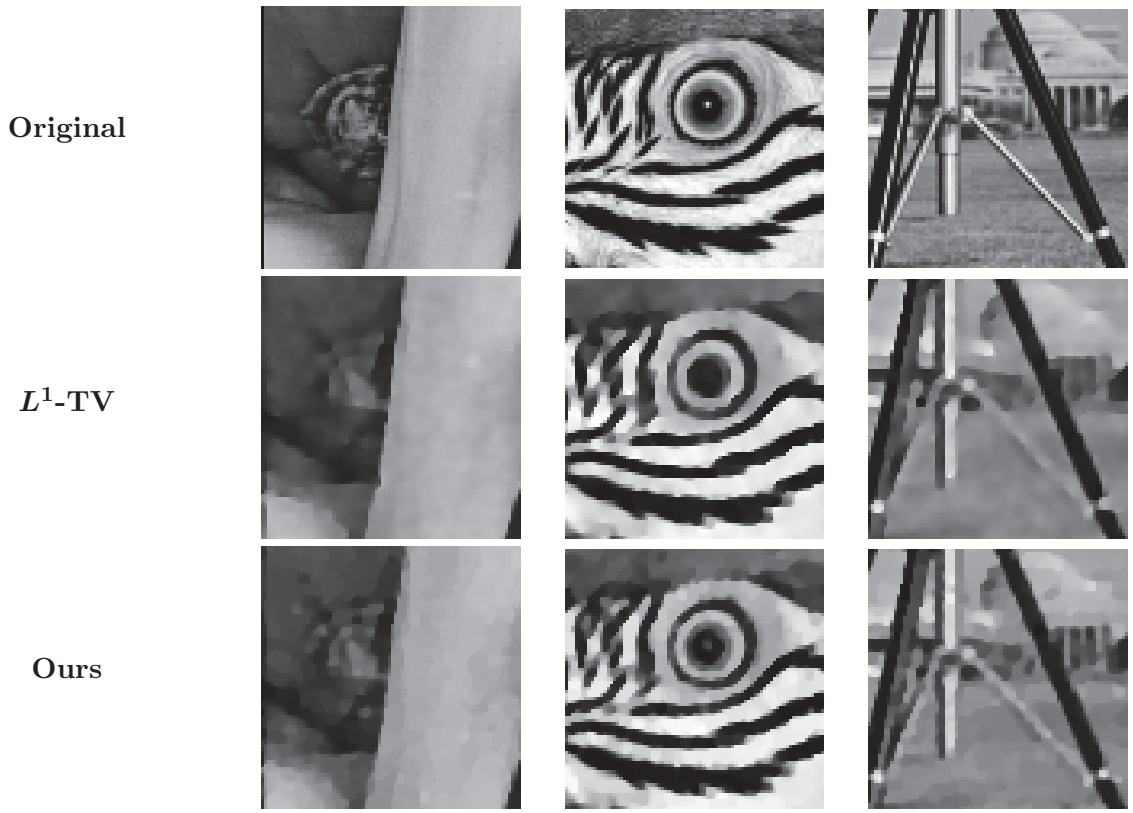

Figure 11. *The zoomed-in regions of the recovered images in Figure 10. First row: details of original images; second row: details of restored images by L^1-TV approach; third row: details of restored images by our approach.*

Table 5

PSNR values for noisy images and recovered images given by different methods ($\xi = 0.02$). In the last line of the table, we compute the average of the values.

	Noisy	ROF	MD	MR	L^1-TV	**Ours**
Peppers	18.31	24.21	25.19	25.01	26.70	**27.46**
Parrot	18.23	24.06	24.48	24.57	25.75	**26.79**
Cameraman	18.29	23.98	24.43	24.39	25.49	**26.27**
Lena	18.64	25.74	26.70	26.72	27.26	**28.14**
Baboon	17.42	20.84	21.54	21.49	21.36	**21.81**
Goldhill	18.47	24.84	25.88	25.85	26.17	**26.76**
Boat	18.48	24.36	25.42	25.43	26.18	**26.69**
Average	18.28	24.00	24.81	24.78	25.56	**26.31**

Now, collecting the term with the same factor γ^2, we have

$$\gamma^2\Big((u_2-f_1)^2+(u_1-f_2)^2-(u_1-f_1)^2-(u_2-f_2)^2\Big)+(u_2-f_1)^2(u_1-f_2)^2-(u_1-f_1)^2(u_2-f_2)^2<0.$$

Table 6

SSIM measures for noisy images and recovered images given by different methods ($\xi = 0.02$). In the last line of the table, we compute the average of the values.

	Noisy	ROF	MD	MR	L^1-TV	**Ours**
Peppers	0.2413	0.4974	0.5909	0.5762	0.6086	**0.6297**
Parrot	0.2316	0.4439	0.5145	0.4991	0.5278	**0.5655**
Cameraman	0.1753	0.2609	0.3433	0.3296	0.3516	**0.3880**
Lena	0.2487	0.4748	0.5764	0.5631	0.5712	**0.6071**
Baboon	0.1955	0.2167	0.3573	0.3502	0.3208	**0.3905**
Goldhill	0.2262	0.3678	0.5070	0.4949	0.4911	**0.5390**
Boat	0.2410	0.4059	0.5313	0.5243	0.5478	**0.5721**
Average	0.2228	0.3811	0.4887	0.4767	0.4884	**0.5274**

The above inequality can be simply rewritten as follows:

$$2\gamma^2(u_1f_1+u_2f_2-u_2f_1-u_1f_2)+\Big(f_1^2u_1^2-2u_1^2u_2f_1+u_2^2f_2^2-2u_2f_1f_2^2-2u_1u_2^2f_2-2u_1f_1^2f_2\Big)\\ -\Big(f_1^2u_2^2-2u_1u_2^2f_1+u_1^2f_2^2-2u_1f_1f_2^2-2u_1^2u_2f_2-2u_2f_1^2f_2\Big)<0,$$

and collecting some terms together we need to prove that

$$2\gamma^2(f_1-f_2)(u_1-u_2)+f_1^2(u_1^2-u_2^2)+f_2^2(u_2^2-u_1^2)\\ +2\Big(-u_1^2u_2f_1-u_2f_1f_2^2-u_1u_2^2f_2-u_1f_1^2f_2+u_1u_2^2f_1+u_1f_1f_2^2+u_1^2u_2f_2+u_2f_1^2f_2\Big)<0.$$

Thus,

$$2\gamma^2(f_1-f_2)(u_1-u_2)+(u_1-u_2)(f_1-f_2)(u_1+u_2)(f_1+f_2)\\ +2\Big(u_1^2u_2(f_2-f_1)+f_1f_2^2(u_1-u_2)+u_1u_2^2(f_1-f_2)+f_1^2f_2(u_2-u_1)\Big)<0$$

and hence

$$2\gamma^2(f_1-f_2)(u_1-u_2)+(u_1-u_2)(f_1-f_2)(u_1+u_2)(f_1+f_2)\\ +2\Big(u_1u_2(u_1-u_2)(f_2-f_1)+f_1f_2(f_2-f_1)(u_1-u_2)\Big)<0.$$

Finally, collecting $(f_1-f_2)(u_1-u_2)$ we need to prove that

$$(f_1-f_2)(u_1-u_2)\Big(2\gamma^2+(u_1+u_2)(f_1+f_2)-2(u_1u_2+f_1f_2)\Big)<0.$$

Hence, since $f_1<f_2$ and $u_1>u_2$, we just need to show that

$$2\gamma^2+(f_1+f_2)(u_1+u_2)-2(f_1f_2+u_1u_2)>0. \tag{A.3}$$

Using the Cauchy inequality, we can easily find that (A.3) is consequence of the following:

$$(\sqrt{u_1u_2} - f_1)(\sqrt{u_1u_2} - f_2) < \gamma^2. \tag{A.4}$$

From Theorem 3.1, we know that $a_1 \le u_1 \le b_1$ and $a_2 \le u_2 \le b_2$; thus, by the hypothesis that $f_1 < f_2$, we have $a_1 < \sqrt{u_1u_2} < b_2$. Furthermore, $|\sqrt{u_1u_2} - f_1| < b_2 - a_1$ and $|\sqrt{u_1u_2} - f_2| < b_2 - a_1$. Hence, the inequality in (A.4) always holds if $(b_2 - a_1)^2 < \gamma^2$, and thus $b_2 < \gamma + a_1$.

Acknowledgment. The authors would like to thank the reviewers for their careful reading of the manuscript and the insightful and constructive comments.

REFERENCES

[1] A. Achim and E. Kuruoğlu, *Image denoising using bivariate K-stable distributions in the complex wavelet domain*, IEEE Signal Process. Lett., 12 (2005), pp. 17–20.
[2] L. Ambrosio, N. Fusco, and D. Pallara, *Functions of Bounded Variation and Free Discontinuity Problem*, Oxford University Press, London, 2000.
[3] G. Aubert and J.-F. Aujol, *A variational approach to removing multiplicative noise*, SIAM J. Appl. Math., 68 (2008), pp. 925–946.
[4] G. Aubert and P. Kornprobst, *Mathematical Problems in Image Processing: Partial Differential Equations and the Calculus of Variations*, Appl. Math. Sci. 147, Springer, New York, 2006.
[5] A. Bovik, *Handbook of Image and Video Processing*, Academic Press, New York, 2000.
[6] S. Boyd, N. Parikh, E. Chu, B. Peleato, and J. Eckstein, *Distributed optimization and statistical learning via the alternating direction method of multipliers*, Found. Trends Mach. Learn., 3 (2010), pp. 1–122.
[7] D. Brownrigg, *The weighted median filter*, Commun. Ass. Comput. Mach., 27 (1984), pp. 807–818.
[8] J. Cai, R. Chan, and Z. Shen, *A framelet-based image inpainting algorithm*, Appl. Comput. Harmon. Anal., 24 (2008), pp. 131–149.
[9] A. Chambolle, *An algorithm for mean curvature motion*, Interfaces Free Bound., 4 (2004), pp. 1–24.
[10] A. Chambolle, *An algorithm for total variation minimization and applications*, J. Math. Imaging Vision, 20 (2004), pp. 89–97.
[11] A. Chambolle and T. Pock, *A first-order primal-dual algorithm for convex problems with applications to imaging*, J. Math. Imaging Vision, 40 (2011), pp. 120–145.
[12] R. Chan, Y. Dong, and M. Hintermüller, *An efficient two-phase L1-TV method for restoring blurred images with impulse noise*, IEEE Trans. Image Process., 19 (2010), pp. 1731–1739.
[13] R. Chan, H. Yang, and T. Zeng, *A two-stage image segmentation method for blurry images with Poisson or multiplicative gamma noise*, SIAM J. Imaging Sci., 7 (2014), pp. 98–127.
[14] T. F. Chan, G. H. Golub, and P. Mulet, *A nonlinear primal-dual method for total variation-based image restoration*, SIAM J. Sci. Comput., 20 (1999), pp. 1964–1977.
[15] T. F. Chan and J. Shen, *Image Processing and Analysis: Variational, PDE, Wavelet, and Stochastic Methods*, SIAM, Philadelphia, 2005.
[16] Y. Chang, S. Kadaba, P. Doerschuk, and S. Gelfand, *Image restoration using recursive Markov random field models driven by Cauchy distributed noise*, IEEE Signal Process. Lett., 8 (2001), pp. 65–66.
[17] L. Condat, *A primal-dual splitting method for convex optimization involving Lipschitzian, proximable and linear composite terms*, J. Optim. Theory Appl., 158 (2013), pp. 460–479.
[18] K. Dabov, A. Foi, V. Katkovnik, and K. Egiazarian, *Image denoising by sparse 3D transform-domain collaborative filtering*, IEEE Trans. Image Process., 16 (2007), pp. 2080–2095.
[19] N. Dey, L. Blanc-Féraud, C. Zimmer, P. Roux, Z. Kam, J. Olivo-Marin, and J. Zerubia, *Richardson-Lucy algorithm with total variation regularization for 3D confocal microscope deconvolution*, Microsc. Res. Tech., 69 (2006), pp. 260–266.
[20] Y. Dong and S. Xu, *A new directional weighted median filter for removal of random-valued impulse noise*, IEEE Signal Process. Lett., 14 (2007), pp. 193–196.

[21] Y. Dong and T. Zeng, *A convex variational model for restoring blurred images with multiplicative noise*, SIAM J. Imaging Sci., 6 (2013), pp. 1598–1625.
[22] M. Elad and M. Aharon, *Image denoising via sparse and redundant representations over learned dictionaries*, IEEE Trans. Image Process., 15 (2006), pp. 3736–3745.
[23] L. Evans, *Partial Differential Equations*, American Mathematical Society, Providence, RI, 2010.
[24] B. Figueiredo and J. Bioucas-Dias, *Restoration of Poissonian images using alternating direction optimization*, IEEE Trans. Image Process., 19 (2010), pp. 3133–3145.
[25] B. Frieden, *A new restoring algorithm for the preferential enhancement of edge gradients*, J. Opt. Soc. Amer., 66 (1976), pp. 116–123.
[26] G. Gilboa and S. Osher, *Nonlocal operators with applications to image processing*, Multiscale Model. Simul., 7 (2008), pp. 1005–1028.
[27] E. Giusti, *Minimal Surfaces and Functions of Bounded Variation*, Birkhäuser Boston, Cambridge, MA, 1984.
[28] T. Goldstein and S. Osher, *The split Bregman method for L1-regularized problems*, SIAM J. Imaging Sci., 2 (2009), pp. 323–343.
[29] J. Gonzalez and G. Arce, *Optimality of the myriad filter in practical impulsive noise environments*, IEEE Trans. Signal Process., 49 (2001), pp. 438–441.
[30] J. Gonzalez and G. Arce, *Weighted myriad filters: A robust filtering framework derived from alpha-table distributions*, in Proceedings of the IEEE International Conference on Acoustics, Speech and Signal Processing (ICASSP), Vol. 5, Atlanta, GA, 1996, pp. 2833–2836.
[31] G. Grimmett and D. Welsh, *Probability: An Introduction*, Oxford Science Publications, London, 1986.
[32] M. El Hassouni and H. Cherifi, *Alpha-stable noise reduction in video sequences*, in Image Analysis and Recognition, A. C. Campilho and M. S. Kamel, eds., Springer, Berlin, 2004, pp. 580–587.
[33] Y. Huang, L. Moisan, M. Ng, and T. Zeng, *Multiplicative noise removal via a learned dictionary*, IEEE Trans. Image Process., 21 (2012), pp. 4534–4543.
[34] Y.-M. Huang, M. K. Ng, and Y.-W. Wen, *A new total variation method for multiplicative noise removal*, SIAM J. Imaging Sci., 2 (2009), pp. 20–40.
[35] H. Hwang and R. Haddad, *Adaptive median filters: New algorithms and results*, IEEE Trans. Image Process., 4 (1995), pp. 499–502.
[36] M. Idan and J. Speyer, *Cauchy estimation for linear scalar systems*, IEEE Trans. Automat. Control, 55 (2010), pp. 1329–1342.
[37] N. Jacobson, *Basic Algebra*, Freeman, New York, 1974.
[38] L. Jacques, L. Duval, C. Chaux, and G. Peyré, *A panorama on multiscale geometric representations, intertwining spatial, directional and frequency selectivity*, Signal Process., 91 (2011), pp. 2699–2730.
[39] B. Kosko, *Noise*, Viking Adult, New York, 2006.
[40] E. Kuruoglu, W. Fitzgerald, and P. Rayner, *Near optimal detection of signals in impulsive noise modeled with asymmetric alpha-stable distribution*, IEEE Commun. Lett., 2 (1998), pp. 282–284.
[41] T. Le, T. Chartrand, and T. Asaki, *A variational approach to reconstructing images corrupted by Poisson noise*, J. Math. Imaging Vision, 27 (2007), pp. 257–263.
[42] H. Lin and A. N. Willson, *Median filter with adaptive length*, IEEE Trans. Circuits Syst., 35 (1988), pp. 675–690.
[43] F. Luisier, T. Blu, and M. Unser, *A new SURE approach to image denoising: Interscale orthonormal wavelet thresholding*, IEEE Trans. Image Process., 16 (2007), pp. 593–606.
[44] L. Ma, M. Ng, J. Yu, and T. Zeng, *Efficient box-constrained TV-type-l^1 algorithms for restoring images with impulse noise*, J. Comput. Math., 31 (2013), pp. 249–270.
[45] M. Nikolova, *Minimizers of cost-functions involving nonsmooth data-fidelity terms. Application to the processing of outliers*, SIAM J. Numer. Anal., 40 (2002), pp. 965–994.
[46] M. Nikolova, *A variational approach to remove outliers and impulse noise*, J. Math. Imaging Vision, 20 (2004), pp. 90–120.
[47] J. Nolan, *Numerical calculation of stable densities and distribution functions*, Comm. Statist. Stochastics Models, 13 (1997), pp. 759–774.
[48] J. Nolan, *Stable Distributions - Models for Heavy Tailed Data*, Birkhäuser Boston, Cambridge, MA, to appear (Chapter 1 available online from http://academic2.american.edu/~jpnolan).
[49] T. Pander, *New polynomial approach to myriad filter computation*, Signal Process., 90 (2010), pp. 1991–

2001.
[50] Y. Peng, J. Chen, X. Xu, and F. Pu, *SAR images statistical modeling and classification based on the mixture of alpha-stable distributions*, Remote Sens., 5 (2013), pp. 2145–2163.
[51] N. Pustelnik, C. Chaux, and J. Pesquet, *Parallel proximal algorithm for image restoration using hybrid regularization*, IEEE Trans. Image Process., 20 (2011), pp. 2450–2462.
[52] P. Reeves, *A Non-Gaussian Turbulence Simulation*, Technical Report AFFDL-TR-69-67, Air Force Flight Dynamics Laboratory, Wright-Patterson Air Force Base, OH, 1969.
[53] L. Rudin, P. Lions, and S. Osher, *Multiplicative denoising and deblurring: Theory and algorithms*, in Geometric Level Sets in Imaging, Vision and Graphics, S. Osher and N. Paragios, eds., Springer, New York, 2003, pp. 103–119.
[54] L. Rudin, S. Osher, and E. Fatemi, *Nonlinear total variation based noise removal algorithms*, Phys. D, 60 (1992), pp. 259–268.
[55] G. Samorodnitsky and M. Taqqu, *Stable Non-Gaussian Random Processes: Stochastic Models with Infinite Variance*, Chapman & Hall, New York, 1994.
[56] S. Setzer, G. Steidl, and T. Teuber, *Deblurring Poissonian images by split Bregman techniques*, J. Visual Commun. Image Represent., 21 (2010), pp. 193–199.
[57] T. Sun and Y. Neuvo, *Detail-preserving median based filters in image processing*, Pattern Recogn. Lett., 15 (1994), pp. 341–347.
[58] C. Sutour, C. Deledalle, and J. Aujol, *Adaptive regularization of the NL-means: Application to image and video denoising*, IEEE Trans. Image Process., 23 (2014), pp. 3506–3521.
[59] T. Wan, N. Canagarajah, and A. Achim, *Segmentation of noisy colour images using Cauchy distribution in the complex wavelet domain*, IET Image Process., 5 (2011), pp. 159–170.
[60] P. Weiss, L. Blanc-Féraud, and G. Aubert, *Efficient schemes for total variation minimization under constraints in image processing*, SIAM J. Sci. Comput., 31 (2009), pp. 2047–2080.
[61] C. Wu and X.-C. Tai, *Augmented Lagrangian method, dual methods, and split Bregman iteration for ROF, vectorial TV, and high order models*, SIAM J. Imaging Sci., 3 (2010), pp. 300–339.
[62] J. Yang, Y. Zhang, and W. Yin, *An efficient TVL1 algorithm for deblurring multichannel images corrupted by impulsive noise*, SIAM J. Sci. Comput., 31 (2009), pp. 2842–2865.
[63] Z. Yang and M. Jacob, *Nonlocal regularization of inverse problems: A unified variational framework*, IEEE Trans. Image Process., 22 (2013), pp. 3192–3203.
[64] W. Zhou, A. Bovik, H. Sheikh, and E. Simoncelli, *Image quality assessment: From error visibility to structural similarity*, IEEE Trans. Image Process., 13 (2004), pp. 600–612.